Second minimum lifetime measurements in ^{133}Nd and ^{137}Nd

S. M. Mullins,* I. Jenkins,† Y-J. He,‡ A. J. Kirwan,§ and P. J. Nolan
Oliver Lodge Laboratory, University of Liverpool, P.O. Box 147 Liverpool L69 3BX, United Kingdom

J. R. Hughes** and R. Wadsworth
Department of Physics, University of York, Heslington, York Y01 5DD, United Kingdom

R. A. Wyss
Joint Institute for Heavy Ion Research, Oak Ridge National Laboratory, P. O. Box 2008, Oak Ridge, Tennessee 37831
(Received 3 September 1991)

The quadrupole moments (Q_0) of the highly deformed, second minimum bands in ^{133}Nd and ^{137}Nd have been extracted from mean lifetime measurements using the Doppler shift attenuation method. The reactions ^{105}Pd(^{32}S,$2p2n$)^{133}Nd at 152 MeV and ^{104}Ru(^{36}S,$3n$)^{137}Nd at 145 MeV were used. A standard centroid shift analysis was carried out in both cases, which gave values of $Q_0=(6.0\pm0.7)e$ b and $(4.0\pm0.5)e$ b for ^{133}Nd and ^{137}Nd, respectively, corresponding to axial prolate deformations of $\beta_2\simeq0.33$ and $\simeq0.22$. A line-shape analysis was also carried out for ^{133}Nd to check against the possible effect of sidefeeding. The result was $Q_0=(6.7+0.7)e$ b, with sightly slower sidefeeding times corresponding to $\overline{Q_{sf}}\simeq5.3e$ b. The results are in good agreement with the predictions of total Routhian surface calculations, and are discussed in the context of other highly deformed bands in the $A=130$–140 mass region.

PACS number(s): 21.10.Tg, 21.10.Re, 27.60.+j

I. INTRODUCTION

The experimental and theoretical study of high angular momentum states in atomic nuclei continues to be a topic of great interest. A certain class of these states originates from the collective rotation of highly deformed shapes predicted by nuclear potential energy surface (PES) calculations. Following on from the fission isomers [1], these shapes are commonly identified with a "second minimum" in the PES, while lower deformation states are associated with the "first minimum," even though many of these nuclei show a number of minima at lower deformations. The deformation associated with the second minimum varies according to the mass region where these high-spin states are observed. Thus, the $A=130$ region is associated with a ~1.5:1 axis ratio (quadrupole deformation $\beta_2\sim0.4$), the $A=150$ region a ~2:1 axis ratio ($\beta_2\sim0.6$), and the $A=190$ region a ~1.65:1 axis ratio ($\beta_2\sim0.5$). Sometimes all three cases are described as "superdeformed," though now it is more common to label the two heavier regions in this way, with the states in the $A=130$ region being called "highly deformed." The aim of the present work was to establish the quadrupole deformations associated with the highly deformed bands observed in ^{133}Nd and ^{137}Nd. This was done by measuring the mean lifetimes of the states in these bands. These were used, in conjunction with the rotational model, to calculate the quadrupole moment (Q_0) from which the quadrupole deformation parameter β_2 was extracted.

Discrete line γ-ray spectroscopy in the second minimum in the $A=130$ region began with ^{132}Ce when a band characterized by a narrow (~70 keV) and fairly regular energy spacing was discovered [2]. The large dynamic moment of inertia [$\mathcal{J}^{(2)}\sim(55$–$60)\hbar^2$ MeV^{-1}] indicated by the narrow energy spacing implied a prolate deformation considerably greater than that of the lower spin bands in ^{132}Ce [3,4], and indeed in other nuclei in the neighboring mass region. This was confirmed when a measurement of the quadrupole moment of the band was performed [5] showing that the deformation was indeed large [$Q_0=(8.8\pm0.8)e$ b, corresponding to $\beta_2\simeq0.5$]. A systematic search of nuclei in the mass region has uncovered a number of bands with similar large moments of inertia. Attention has now focused on the detailed properties of these bands. If the bands are associated with an underlying symmetry of the deformed field, then one would expect them to have similar deformations. The deformed harmonic oscillator potential, for instance, shows gaps at a 3:2 axis ratio for many particle numbers relevant to the $A=130$–140 region. If the particular single-particle configuration, however, is the dominant

*Present address: Dept. of Physics, McMaster University, Hamilton, Ontario, Canada L8S 4M1.
†Present address: AEA Technology, Culham Laboratory, Abingdon, Oxon, U.K.
‡Present address: Dept. of Physics, National University of Singapore, Singapore 0511.
§Present address: SRD, Culcheth, Warrington, WA3 4NE U.K.
**Present address: Dept. of Physics, SUNY, Stony Brook, NY 11794.

deformation driving force then one would expect to see differences in deformation and structure when going from nucleus to nucleus. Since, in general, transitions linking the bands to known states have not been found, the spins (and excitation energies) are undetermined. The $\mathcal{J}^{(2)}$ dynamic moment of inertia, however, does not depend on spin, and can be readily extracted from the differences between adjacent transition energies. The behavior of $\mathcal{J}^{(2)}$ as a function of rotational frequency is sensitive to the number high-N_{osc} (N_{osc} is the major oscillator quantum number) intruder orbitals which are occupied. Any band crossings, alignments, or changes in pairing also show up very clearly in the $\mathcal{J}^{(2)}$. For instance, in the two even-N cases ^{132}Ce and ^{136}Nd, the $\mathcal{J}^{(2)}$'s are very similar, while in the odd-N cases there are large variations. This suggests that there are important structural differences between the even- and odd-N cases. The proximity of the active orbitals relative to the Fermi surface has a sensitive dependence on deformation. Thus, if one is to have any hope of understanding the intrinsic structure of these bands, a reliable measurement of the quadrupole deformation is needed. This is best accomplished by measuring the lifetimes within these bands, in order to extract the quadrupole moment. Measurements of quadrupole moments have therefore been undertaken in as many cases as possible. Since the initial case of ^{132}Ce, results have been published for ^{131}Ce [6], ^{135}Nd [7], ^{135}Sm [8], and ^{139}Gd [9]. The results for ^{133}Nd and ^{137}Nd will be presented here.

II. EXPERIMENTAL DETAILS

The Doppler shift attenuation method (DSAM) [10] was used to measure the average recoil velocities at which the highly deformed states in ^{133}Nd and ^{137}Nd decayed. The reactions used were ^{105}Pd(^{32}S,2p2n)^{133}Nd at 152 MeV with the ESSA30 spectrometer [11], and ^{104}Ru(^{36}S,3n)^{137}Nd at 145 MeV with TESSA3 [12]. Both arrays make use of Compton suppressed high-purity n-type germanium detectors. The thirty detectors of ESSA30 were grouped into six sets of five at angles of 37°, 63°, 79°, 101°, 117°, and 143° with respect to the beam direction. The sixteen detectors of TESSA3 were grouped into three sets of four at 35°, 90°, and 145°, plus two sets of two at 60° and 120°. TESSA3 also has a fifty-element bismuth germanate (BGO) inner ball from which sum-energy (total energy deposited) and fold (number of elements which fire) information was obtained. In both cases a target of $\sim 500\ \mu g/cm^2$ thickness was used, mounted on a $\sim 10\text{-mg/cm}^2$ ^{197}Au backing. Self-supporting targets (also of $\sim 500\ \mu g/cm^2$ thickness) were used before commencing the DSAM experiments. Approximately 500×10^6 γ-γ (and higher-fold) events were collected for ^{133}Nd using the backed target, and $\sim 200\times10^6$ events were obtained from the unbacked target. In the case of ^{137}Nd, in excess of 200×10^6 γ-γ-BGO coincidences were written to tape for both the backed and self-supporting targets. In each experiment a ^{152}Eu source was used for the purpose of energy and efficiency calibration, and for gain matching the detectors to fully stopped transitions for the DSAM analysis.

III. DATA ANALYSIS AND RESULTS

The DSAM data were replayed offline into γ-γ coincidence matrices for the purpose of producing spectra containing counts from only one specific detector group. This enabled Doppler shifts at one particular angle to be measured. The shifts were measured for the most forward and backward detector groups, since the Doppler effect was largest at these angles. Thus, in the case of ESSA30, the angles used were 37° and 143°, and for TESSA3, 35° and 145°. The sum-energy/fold information from the TESSA3 BGO ball was used to preferentially select events belonging to ^{137}Nd over those from the $4n$(^{136}Nd) and $5n$(^{135}Nd) channels. No such selection was possible for the ESSA30 data. The matrices were constructed so that events where at least one detector at the required angle (e.g., 37°) fired were stored. This was done in two ways. The first method selected coincidences between any detector at the required angle with a detector at another specific angle. Thus, for 37° in ESSA30, for example, matrices were constructed for 37° versus 37°, 37° versus 63°, 37° versus 79°, and so on. The same procedure was carried out for 143°, and, in the case of TESSA3, for the 35° and 145° detectors. The second method selected coincidences between detectors at the required angle with any other detector, regardless of angle. Hence, only two matrices were needed for each data set:

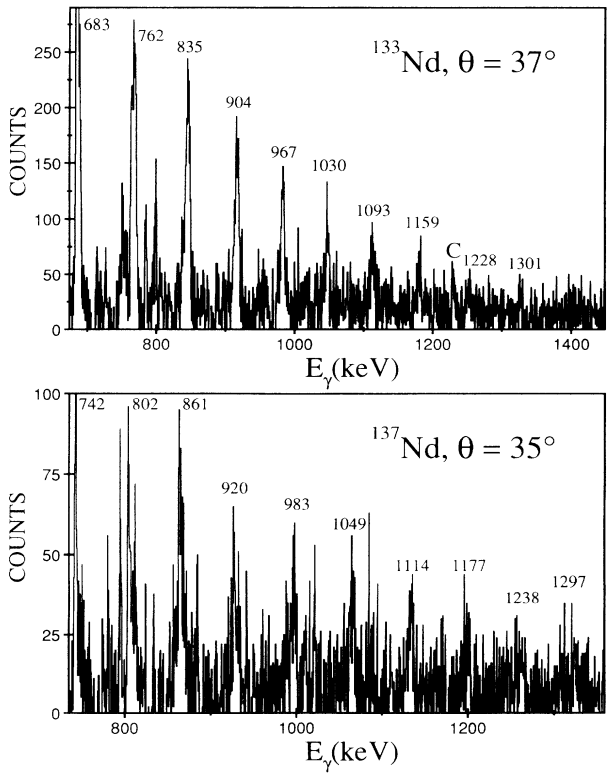

FIG. 1. Partial spectra showing Doppler shifted γ rays at 37° for ^{133}Nd and 35° for ^{137}Nd, produced as described in the text. The peaks have been labeled with the unshifted transition energy; the peak near the 1228-keV γ ray in ^{133}Nd labeled C is from Coulomb excitation of the ^{105}Pd target.

37° versus "all angles" and 143° versus "all angles" for ESSA30, and 35° versus "all angles" and 145° versus "all angles" for TESSA3. The former method made it possible to gate on both unshifted and shifted transitions, whereas the latter technique restricts one to slicing on unshifted lines only.

The lowest four inband γ rays in ^{133}Nd (409, 441, 513, and 603 keV [13,14]) were found to have decayed after the nuclei had fully stopped (i.e., showed no Doppler shift), as did the 344-keV dipole transition which feeds out from the bottom of the band. This was also the case for the bottom three transitions (635, 679, and 742 keV [13,15]) in ^{137}Nd. The best spectra for ^{133}Nd were produced by summing gates set on all the "stopped" transitions listed above, barring the 409-keV γ ray as this introduced too many contaminant lines. Gating on "moving" transitions (i.e., those which showed a Doppler shift) was tried in order to eliminate the effect of sidefeeding on the transitions below, but the resultant spectra did not have sufficient counts to make this worthwhile. Similarly for ^{137}Nd, gates were set on the stopped peaks and also on the partially shifted 804-keV γ ray. Partial forward angle spectra for both nuclei are shown in Fig. 1.

A. Centroid shift analysis

The centroid shift technique is concerned only with average quantities, in particular comparing the average recoil velocity at which a state decays with the average initial recoil velocity at which the nuclei were produced. This was done by measuring the centroids of the Doppler-shifted peaks from the forward and backward spectra. The energy shift (ΔE_γ) from the unshifted energy [$E_\gamma(0)$] was then extracted for each transition and converted to an average recoil velocity using the standard (first-order) Doppler-shift formula. These were converted to $F(\tau)$ factors by dividing by the average initial recoil velocities calculated from kinematics ($\langle v_0 \rangle / c = 2.33\%$ for ^{133}Nd and 2.38% for ^{137}Nd assuming production at the middle of the target). The $F(\tau)$ data points are shown in the lower part of Fig. 2. The error bars reflect the uncertainties in determining the centroids, including such factors as placement of peak markers and different background fitting. Also shown in Fig. 2 are theoretical curves produced from combining the assumption a rotational cascade of constant quadrupole moment with a stopping calculation for the particular recoiling nuclei. This is the standard method for relating decay time to recoil velocity for superdeformed bands. The code FTAU [16] was used to model the slowing down of the recoils. The electronic and nuclear stopping powers of Braune [17] were used, which are claimed to be accurate to ~10% over the range of recoil velocities involved here. The stopping powers of Ziegler [18] are not claimed to be reliable for recoil energies less than 0.22 MeV per nucleon [19], which corresponds to recoil velocities of $v/c \sim 2.2\%$ for the present cases. In terms of $F(\tau)$, this limit translates to $F(\tau) \sim 0.93$ and 0.91 for ^{133}Nd and ^{137}Nd, respectively. Hence a comparison with Fig. 2 shows that all the data points (with the exception of the topmost one for ^{133}Nd) fall below this limit. Above this limit, however, the two stopping powers do give very similar results. The Blaugrund [20] method was used to calculate the average large-angle scattering out of the initial recoil direction as a result of the nuclear collisions. This formalism has been regarded as adequate for centroid shift analysis [10]. Feeding corrections were calculated by solving the Bateman equations embodied in the code FFEED [16]. Sidefeeding times have been assumed to have the same profile as the inband feeding. The amount of sidefeeding is indicated in the upper part of Fig. 2, where the relative intensities of the band members are shown from using the unbacked target data. The gating transitions were the same as those used for the backed target data in order to obtain the correct feeding patterns for the lifetime analysis. Comparison of the data with the Q_0 curves indicate that values of $(6.0 \pm 0.7)e$ b for ^{133}Nd and $(4.0 \pm 0.5)e$ b for ^{137}Nd give the best fits. The errors are mainly due to the uncertainties in the stopping powers.

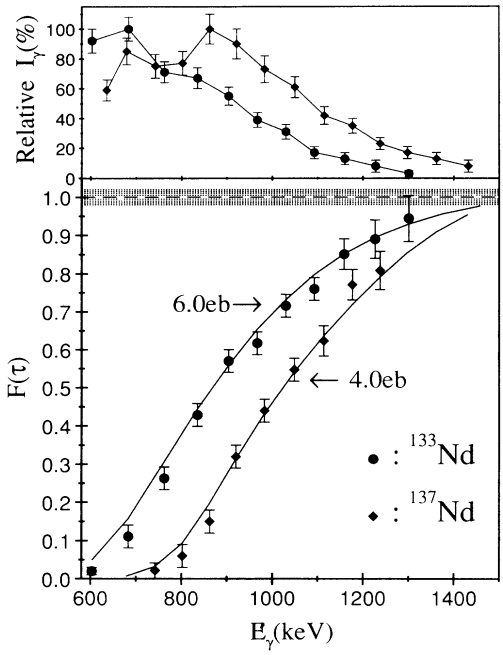

FIG. 2. Bottom: Experimental $F(\tau)$ values extracted from the Doppler-shifted peaks. The dotted region indicates the estimates spread in initial recoil velocity due to the ~500-μg/cm^2 thickness of the targets used in the experiments. The curves assume a single cascade which has a constant quadrupole moment. Any sidefeeding has been assumed to have the same time structure as the inband feeding. Top: Feeding patterns from the unbacked target data. These show the relative intensities of the in-band transitions when gating on the same transitions as were used in the backed target data.

B. Line-shape analysis for ^{133}Nd

In the determination of Q_0 for ^{135}Nd reported in [7], both a centroid shift and a full line-shape analysis were carried out. The line-shape analysis indicated that the centroid shift analysis was unreliable due to the sidefeeding times being much slower. The centroid shift technique gave a result of $Q_0 = 5.4e$ b, whereas the line-shape

fitting gave $Q_0=(7.4\pm1.0)e$ b, with an average sidefeeding Q_0 of $3.5e$ b. Hence the Q_0 arrived at from the line-shape analysis was much larger than the centroid shift value. Here, a line-shape analysis has been carried out for ^{133}Nd, since not only is the band significantly more intense ($\sim$20% relative to the total channel intensity) than the band in ^{137}Nd ($\sim$12%), but also twice as many events had been collected. It was therefore doubtful that the data for ^{137}Nd had adequate statistics for a reliable line-shape analysis.

The set of codes used in the ^{135}Nd analysis [7], originally developed by [21] but now modified, were employed here. An array of velocity profiles (theoretical line shapes) were generated by projecting a set of 5000 Monte Carlo histories (simulated collision paths) in $\sim$1.2 fs time steps towards the specified detector configurations at 37° and 143°. The histories were produced by the first program in the set (this had been modified from the original with which there had been a slight problem concerning the stopping powers as discussed in [22]). The electronic stopping powers of Braune were used, together with the Lindhard formalism [23] for the nuclear stopping. A Monte Carlo algorithm was used to find the scattering angle and the magnitude of the energy loss at each collision. On average, the recoiling nuclei were fully stopped after $\sim$ 1.3 ps. Line shapes were then generated from the array of velocity profiles by specifying the Q_0 of the band at each level, the sidefeeding intensity into each state and the Q_0 of the sidefeeding cascade ("Q_{sf}"). The sidefeeding cascade was taken to have the same moment of inertia as the main band, and a $\sim$5 fs feeding time into the band was modeled by adding a fictitious transition on top of the highest level. The total feeding was then treated by solving the Bateman equations. Fits were then made simultaneously to the forward and backward line shapes under the assumption that Q_0 remained constant for the entire band. As a first step an attempt was made to fit the line shapes by fixing $Q_0=Q_{sf}=6.0e$ b (the optimum value from the centroid shift analysis). These fits were generally quite good, though they began to worsen for the two slower transitions below the 835-keV γ ray (the 762- and 683-keV γ rays). This is probably indicated in Fig. 2 by the Q_0 curve missing the corresponding two $F(\tau)$ points. It was not possible to improve the fits by letting Q_0 vary while also maintaining that $Q_{sf}=Q_0$. The higher transitions above the 1030-keV γ ray were not very sensitive to changing Q_0 by $(1-2)e$ b. As a next step, Q_0 and Q_{sf} were allowed to vary independently. This improved the fits greatly, giving values of $Q_0=6.7e$ b and $Q_{sf}=5.3e$ b. Allowing Q_{sf} to vary going down the band did not significantly alter this value of Q_0—optimum values of $Q_{sf}=5.9e$ b at high spin decreasing to $5.3e$ b at lower spin were found. This indicates the insensitivity of the higher transitions to rather large changes in Q_{sf}, as well as Q_0. The fitted line shapes for the 683-, 762-, 835-, and 904-keV transitions are shown in Fig. 3. This suggests that the sidefeeding is up to $\sim$1.6 times slower than the in-band feeding, which is a very similar result to that found for the superdeformed band in ^{192}Hg [24]. Consequently, for ^{133}Nd the result from the centroid shift analysis agrees within errors with that found from the line-shape fitting.

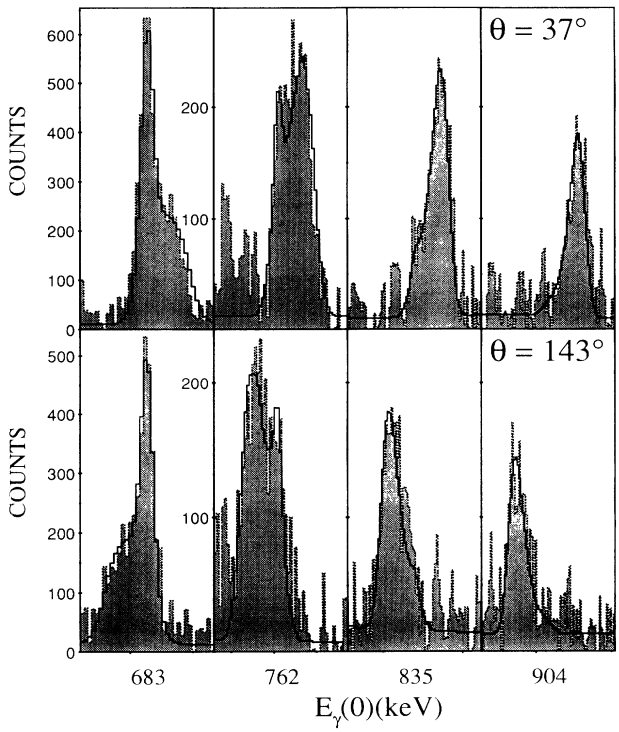

FIG. 3. Comparison of calculated line shapes (solid lines) with experiment (dotted lines and shaded-in area) for the 683-, 762-, 835-, and 904-keV transitions in ^{133}Nd. Details of how the fits were produced are described in the text. Transitions below 683 keV were fully stopped, and hence displayed no line shape, while those above 904 keV were relatively insensitive to the fitting procedure.

IV. DISCUSSION

A. Deformation systematics

A "superdeformed" nucleus is conventionally associated with a strongly elongated prolate shape, with the quadrupole deformation term generally dominating

TABLE I. Quadrupole moments and deformation parameters for the highly deformed bands in the $A=130-140$ region. For consistency, Braune stopping powers have been used in all cases (except ^{135}Nd), including ^{132}Ce (the result published in [5] used a different set of stopping powers).

Nucleus $^A_Z X_N$	Q_0 (e b), β_2 ($\gamma=0°$) Centroid shift	Line-shape fit
$^{131}_{58}Ce_{73}$	6.0(0.6), 0.35(0.04)	not available
$^{132}_{58}Ce_{74}$	7.5(0.6), 0.43(0.04)	not available
$^{133}_{60}Nd_{73}$	6.0(0.7), 0.33(0.03)	6.7(0.7), 0.37(0.04)
$^{135}_{60}Nd_{75}$	5.4(1.0), 0.29(0.03)	7.4(1.0), 0.41(0.05)
$^{137}_{60}Nd_{77}$	4.0(0.5), 0.22(0.03)	not available
$^{135}_{62}Sm_{73}$	7.0(0.7), 0.34(0.04)	6.2(0.6), 0.30(0.03)
$^{137}_{62}Sm_{75}$	5.0(0.7), 0.27(0.03)	not available
$^{139}_{64}Gd_{75}$	7.0(1.5), 0.35(0.07)	no unique value

higher-order distortions. Any deviation away from axiality is generally thought to be negligible for the cases studied thus far. A uniform charge density and sharp surface are also assumed. The generally good agreement between deformations inferred from the $\mathcal{J}^{(2)}$ moments of inertia and those extracted from the quadrupole moments suggests that this is reasonable. Under these assumptions, and a quadrupoloidal parametrization of the nuclear shape [25], deformations have been extracted for ^{133}Nd and ^{137}Nd from the quadrupole moments. The results are summarized in Table I, together with those for the other highly deformed bands in the $A=130-140$ mass region. The discussion below focusses on the trends in deformation as a function of neutron number, with particular attention being given to the odd-N Nd isotopes.

1. $N=73$ isotones

The centroid shift result for ^{133}Nd corresponds to a deformation parameter of $\beta_2 \simeq 0.33$, whereas the line-shape analysis gives a slightly larger value of $\beta_2 \simeq 0.37$. Shown in Fig. 4 are the results of total Routhian surface (TRS) calculations at four rotational frequencies. At $\hbar\omega=0.292$ MeV (corresponding roughly to a spin of $15\hbar$) a prolate minimum with $\beta_2=0.358$ can be seen, which decreases to $\beta_2=0.322$ at $\hbar\omega=0.703$ MeV. Hence, on average the agreement with the experimental deformation is very good.

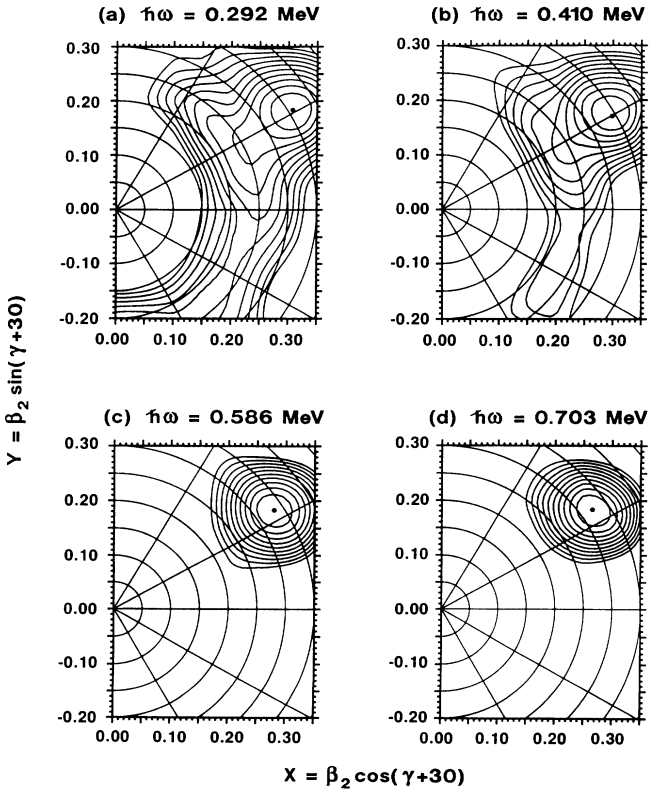

FIG. 4. Total Routhian surface (TRS) calculations for the lowest $(\pi,\alpha)=(+,+\frac{1}{2})$ configuration in ^{133}Nd at four rotational frequencies.

Calculations based on either a Nilsson [26] or a Woods-Saxon [27] potential predict that the first available $i_{13/2}$ neutron orbital is occupied for $N=73$. This is the $\alpha=+\frac{1}{2}$ signature, stemming from the $i_{13/2}[660]\frac{1}{2}^+$ Nilsson orbital. This orbital has a strongly down-sloping trajectory in the Nilsson diagram, so that its position relative to the Fermi surface has a very sensitive dependence on the deformation. Moreover, occupancy of this orbital is responsible for the enhanced deformations of these bands, since the deformation drive is proportional to the negative slope. This suggests that the bands in the $N=73$ isotones should have very similar deformations. This is indeed found to be the case when one compares with the other $N=73$ isotones, namely ^{131}Ce ($\beta_2 \simeq 0.35$ [6]) and ^{135}Sm ($\beta_2 \simeq 0.34$ [8]). The other $N=73$ case is ^{130}La [28] which is the only odd proton nucleus with a highly deformed band in the $A=130-140$ region. An attempt has been made to measure the quadrupole moment of this band, but no result was forthcoming due to difficulties with the target used in the experiment.

2. $N=75$ isotones

The addition of two more neutrons to ^{133}Nd allows for the possibility of occupying the next $i_{13/2}$ orbital. If this orbital is occupied, then the additional deformation drive would suggest that ^{135}Nd should be more deformed than ^{133}Nd. The odd neutron would then occupy either an $h_{11/2}$ or $h_{9/2}$ orbital, giving the band negative parity. If not, then both of the two additional neutrons will occupy non-β_2-driving orbitals coming from either the $h_{11/2}$ or $h_{9/2}$ shell. Calculations using the Nilsson model [26] do not rule out either possibility, whereas those using the Woods-Saxon model [27] indicate that the second $i_{13/2}$ orbital is not occupied.

Shown in Fig. 5 are TRS calculations for ^{135}Nd. These show a prolate minimum with $\beta_2=0.32-0.31$ over the range of rotational frequencies where the band is observed in this nucleus. When compared to ^{133}Nd (Fig. 4), the minimum does not dominate the surface so clearly, and it is no longer yrast at $\hbar\omega=0.292$ MeV. Moreover, a slightly smaller deformation than ^{133}Nd is predicted, since the deformation drive of the $i_{13/2}$ orbital is lessened as it is now closer to the Fermi surface. The experimental deformations taken from the centroid shift analyses are in agreement with this prediction, but the full line-shape analyses give ^{135}Nd a somewhat larger deformation ($\beta_2 \simeq 0.41$, $Q_0=7.4e$ b [7]) than ^{133}Nd ($\beta_2 \simeq 0.37$, $Q_0=6.7e$ b). This value of β_2 for ^{135}Nd is much larger than the average β_2 predicted by the TRS calculations, and strongly suggests that the second $i_{13/2}$ neutron orbital is occupied. The occupancy of two $i_{13/2}$ orbitals would be expected to give rise to a band crossing at the point where this pair of neutrons dealign. Cranked shell model calculations predict that the crossing frequency should be $\hbar\omega \simeq 0.4$ MeV. Such a feature is seen in ^{132}Ce ($N=74$), where the $\mathcal{J}^{(2)}$ moment of inertia increases strongly with decreasing spin, whereupon the band decays back to the "normal states" at a frequency of 0.4 MeV/$\hbar$. Similar behavior is seen in ^{136}Nd [29] ($N=76$). The $\mathcal{J}^{(2)}$ moment of inertia for ^{135}Nd (see Fig. 7), however, does not show this

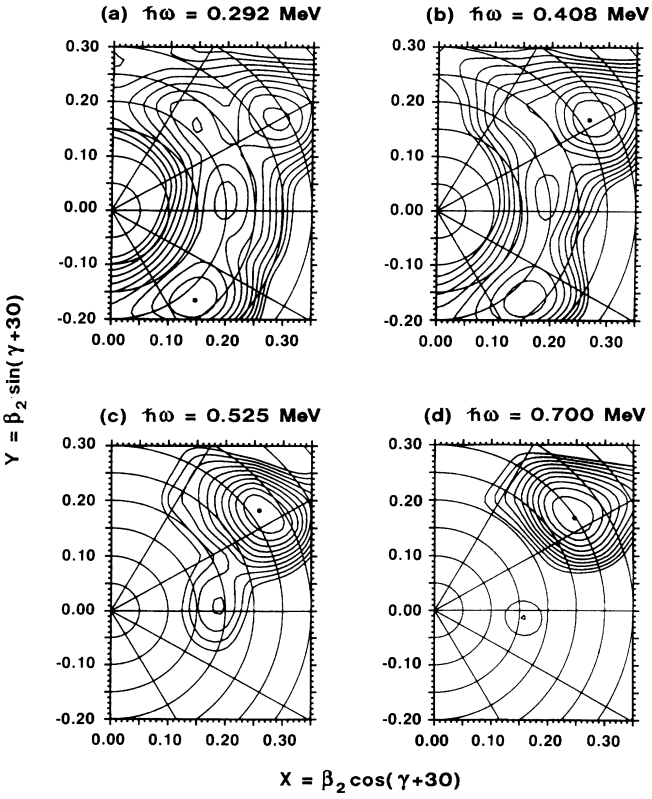

FIG. 5. TRS calculations (as Fig. 4) but for ^{135}Nd.

feature, and the band continues down to a much lower rotational frequency, indicating that this crossing is blocked. Hence this feature suggests that only one $i_{13/2}$ orbital is occupied, and is difficult to reconcile with the large value of β_2 mentioned above.

The two other $N=75$ isotones listed in Table I are ^{137}Sm and ^{139}Gd. Comparison of the centroid shift results only indicate that ^{135}Nd and ^{137}Sm have very similar quadrupole moments, while that of ^{139}Gd is considerably larger. The line-shape analysis for ^{139}Gd was not able to give a unique result, and the data for ^{137}Sm were not of sufficient statistical quality for this procedure to be carried out reliably. It is possible, therefore, that like ^{135}Nd these results may increase if a reliable line-shape analysis shows that there is slow side feeding. It may be, however, that unlike $N=73$ there is no common deformation for $N=75$, which might indicate that there are differences in the number of $i_{13/2}$ neutron orbitals occupied among the $N=75$ bands. Indeed, a decoupled band in the lighter $N=75$ isotone, ^{133}Ce [30], initially assigned as having a $(\nu i_{13/2})^1$ component, clearly does not have such, since a DSAM measurement has shown the quadrupole moment to be only $\sim 2.3e$ b [31].

3. *N = 77 isotones*

The deformation extracted for ^{137}Nd is $\beta_2 \simeq 0.22$, which is much lower than either ^{133}Nd or ^{135}Nd. This may be due to the assumption of an axial prolate shape being incorrect. Total Routhian surface (TRS) calculations for ^{137}Nd are shown in Fig. 6, where a triaxial minimum ($\beta_2 = 0.27$–0.29 and $\gamma \sim 10°$–$20°$) can be seen at high rotational frequencies. The shape change towards positive γ is caused by the alignment of $h_{9/2}$ neutrons, which would be responsible for the second hump in the $\mathcal{J}^{(2)}$ moment of inertia (see Fig. 7), the first being due to the alignment of $h_{11/2}$ protons. This moves into a prolate minimum as the frequency decreases. Both minima are rather soft. Since

$$Q_0 \propto \beta_2 \cos(\gamma + 30°) ,$$

positive values of γ reduce Q_0 for a given β_2. The triaxial shape from the TRS corresponds to a quadrupole moment of $\sim(3.5$–$4.0)e$ b, which is in good agreement with the experimental value. Below the band crossing, a rather larger quadrupole moment would be expected ($Q_0 \simeq 5.3e$ b) since the shape is now prolate. The data suggest that there is no dramatic shape change through the crossing, since a constant Q_0 does quite well in reproducing the measured centroid shifts. It should be noted, however, that the presence of any slow sidefeeding will reduce the measured value of Q_0 and hence β_2 extracted from the centroid shift analysis. The line-shape analysis of ^{133}Nd demonstrated the relative insensitivity of the higher transitions to slow sidefeeding, with only the lower transitions being noticeably effected. It is possible that the corresponding transitions in ^{137}Nd, i.e., those below the band crossing, are being affected by slow sidefeeding. Since the present data are not of sufficient

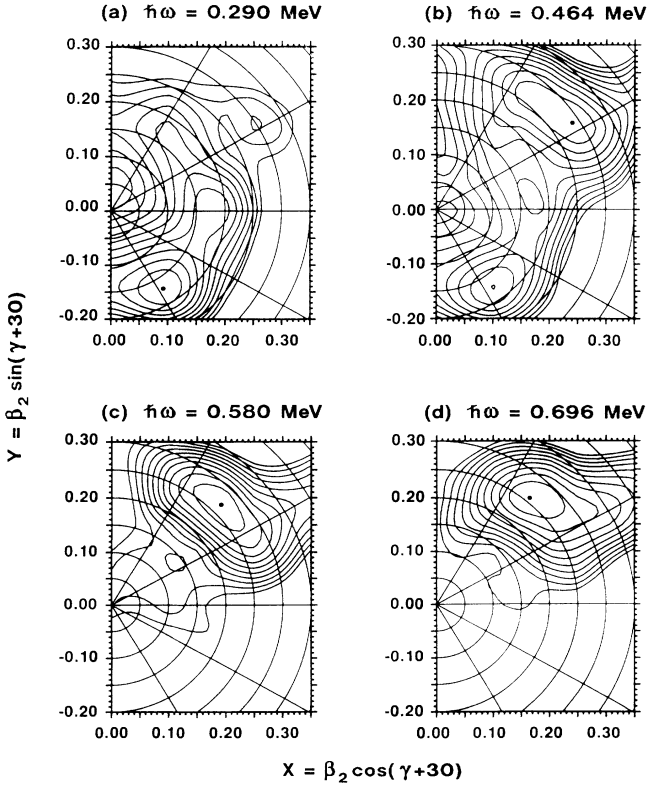

FIG. 6. TRS calculations (as Fig. 4) but for ^{137}Nd.

statistical quality to check against this by using a line-shape analysis, it is possible that the Q_0 for this portion of the band in ^{137}Nd may be rather higher than 4.0e b. It is hoped that a larger data set will be obtained at a future date in order to enable a line-shape analysis to be carried out.

Since the neutron Fermi surface is above midshell, strongly coupled bands are expected for prolate deformations. One may then ask if there are other orbitals which would give rise to decoupled bands. The TRS calculations also show a triaxial minimum with negative γ ($\beta_2=0.17$, $\gamma\simeq-85°$). At negative values of γ, a decoupled band would result, for instance, from a high-K $h_{11/2}$ neutron. The quadrupole moment for this shape would be less than 2e b, and hence can be ruled out by the experimental result. This kind of shape may explain, however, the low quadrupole moment found for the band in ^{133}Ce discussed above.

Another possibility would be the occupancy of the $h_{9/2}[541]\frac{1}{2}^-$ orbital. This configuration is calculated to have a prolate shape with a deformation of $\beta_2=0.20$, which agrees well with the measured quadrupole moment. Even though one would probably expect this kind of band to continue to lower spin than is observed, this possibility cannot be discounted on the basis of the present data.

A high-spin study of the $N=77$ nucleus ^{141}Gd has recently been carried out. A cascade has been assigned to this nucleus, with characteristics very similar to those of the band in ^{137}Nd. Preliminary results suggest that the new band has a similar structure and deformation. These results will appear in a forthcoming publication [32].

4. *Even-N cases*

In the even-N cases, both Nilsson and Woods-Saxon calculations predict that the second $i_{13/2}$ orbital ($\alpha=-\frac{1}{2}$) is occupied. The larger deformation of ^{132}Ce ($N=74$) when compared with ^{131}Ce ($N=73$) suggests that this is true. Clearly it would be of interest to attempt a Q_0 measurement in another even-N case. The best possibility would be ^{136}Nd [29], though the band is quite weak; the existence of the even weaker band in ^{134}Nd [13,29] is somewhat tentative since it has very similar transition energies to the band in ^{131}Ce, as noted by [33].

The TRS calculations also predict excited $i_{13/2}\otimes h_{9/2}$ two-quasineutron configurations to be very favored. These would resemble the highly deformed bands in the odd-N nuclei. No excited bands, however, have thus far been found in the second minima in even-N nuclei in this mass region.

5. *Dynamic moments of inertia of odd-N Nd isotopes*

In Fig. 7 are shown the $\mathcal{J}^{(2)}$ dynamic moments of inertia for ^{133}Nd, ^{135}Nd, and ^{137}Nd. They all show a low-frequency irregularity, where the $\mathcal{J}^{(2)}$ rises extremely rapidly. This common feature is believed to be associated with the decay back to the "normal deformed" states, possibly induced by a dealignment of a pair of $h_{11/2}$ protons. Standard cranking calculations, however, predict

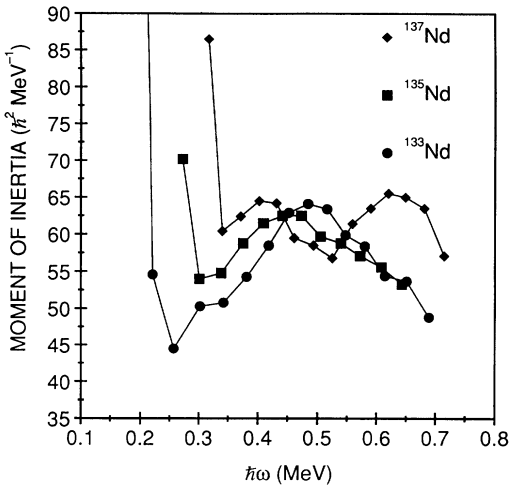

FIG. 7. Dynamic moments of inertia for ^{133}Nd, ^{135}Nd, and ^{137}Nd plotted versus rotational frequency. See text for discussion of these plots.

that this should occur at higher rotational frequencies. Similar irregularities have been observed in $i_{13/2}$ proton bands (e.g., ^{173}Re [34]), which have been interpreted as originating from the mixing of the intruder state with the "normal" states. This allows for a fast decay out of the band. An alternative explanation for this behavior in the highly deformed bands in odd-N nuclei in the $A\simeq135$ region has been put forward in [8]. It is suggested there that the irregularity is due to the onset of proton pairing. The presence of the rotationally aligned low-K, high-j neutron intruder may lead to a serious quenching of the proton pairing through a strong residual n-p interaction. In this scenario there is no change in the number of occupied $h_{11/2}$ proton orbitals; rather the occupancy becomes less sharp in the paired system.

A second common feature is the humplike structure where the $\mathcal{J}^{(2)}$ increases to maximum, and then decreases. The hump, in the first scenario mentioned above, could be associated with a pair of aligned $h_{11/2}$ protons. The second scenario would require that neutron alignments are responsible. As noted in [8], the $\mathcal{J}^{(2)}$ moments of inertia can be reproduced equally well in either scenario. The frequency at which the maximum occurs decreases with increasing neutron number. This is what would be expected if the deformation decreases with increasing neutron number.

A third feature is common only to ^{137}Nd, namely, the second hump beyond $\hbar\omega\simeq0.5$ MeV. The rise to the maximum of the hump has been previously shown [13]; now we are able to show that the $\mathcal{J}^{(2)}$ decreases after this point, since the analysis of the self-supporting target data added two new transitions (1361 and 1431 keV) to the top of the band. As discussed earlier, this feature suggests the presence of a second band crossing or alignment which does not occur in the two lighter Nd isotopes. Cranked shell model (CSM) calculations indicate that alignments of $h_{9/2}$ and $h_{11/2}$ quasineutrons are responsible. Both alignments are predicted to occur simultaneously at $\hbar\omega\simeq0.55$ MeV for a prolate shape, while a posi-

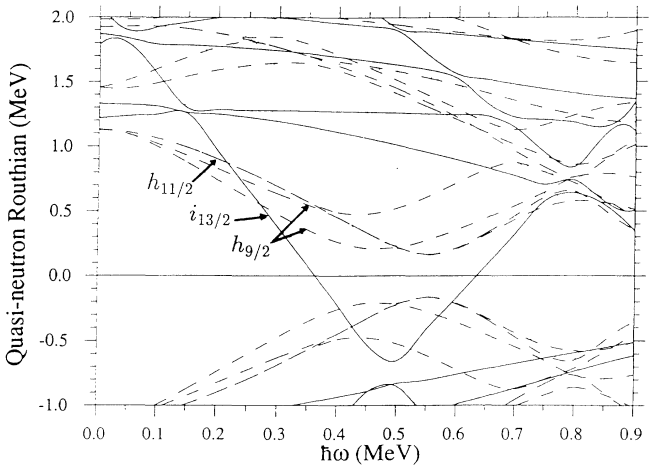

FIG. 8. Cranked shell model (CSM) calculations appropriate for ^{137}Nd, showing quasineutron Routhians. The parameters used were $\beta_2=0.27$, $\gamma=15°$, $\beta_4=0.012$. The Routhians are displayed according to the conserved parity (π) and signature (α) quantum numbers. These are denoted by $(\pi,\alpha)=(+,+\frac{1}{2})$ solid, $(+,-\frac{1}{2})$ dotted, $(-,-\frac{1}{2})$ dashed, $(-+\frac{1}{2})$ dash-dotted lines.

tive (negative) triaxiality γ lowers the frequency of the $h_{9/2}$ ($h_{11/2}$) crossing. The positive γ case is shown in Fig. 8.

B. Line shapes and sidefeeding

Line-shape fitting has now also been applied to the ^{135}Sm data described in [8], and slightly slower sidefeeding times are indicated by the analysis [35]. The line-shape analysis for ^{135}Nd [7] indicated much slower feeding times—around a factor of four slower than the inband times. A similar result has recently been found for ^{139}Gd [9]. This raises the question as to the nature of sidefeeding into these bands, and whether the models used in the analyses are forcing a systematic need for slower sidefeeding times. It could also be that the treatment of the nuclear stopping, which becomes increasingly important for the "slower" transitions (i.e., those which are also the most sensitive to sidefeeding), is inadequate. One may then have to compensate for this by introducing slower sidefeeding to achieve reasonable fits to the line shapes. Assuming that both the sidefeeding and the nuclear stopping are being dealt with adequately, then possible explanations need to be sought for as to why the sidefeeding is slower than the inband feeding, and why it is much slower in some particular cases. If the sidefeeding proceeds via states which are a myriad of nonyrast superdeformed bands, then one would expect the inband transition rates to be "fast," but not so fast as to significantly hinder the approach to the yrast line through decays out of these bands. The sidefeeding into the yrast states may then be a little slower than the cascade feeding down the yrast band. Mixing with "normal deformed" states would also delay feeding times across the continuum, as discussed in [36]. The slightly slower sidefeeding times in ^{133}Nd, ^{192}Hg, and ^{135}Sm may indicate this kind of structure. If noncollective states coexist above the yrast line at high spin, then much slower sidefeeding times are possible, and this might explain the results for ^{135}Nd and ^{139}Gd. Discrete coexisting collective and noncollective high-spin states have recently been found in lighter $A\sim120$ nuclei [37–39], but there is as yet no evidence for similar behavior around $A\sim135$.

It is perhaps worth noting that, despite these bands having in some cases ~10–$20\,\%$ of the channel intensity, they only have barely adequate statistics for a line-shape analysis when compared to "normal deformed" yrast and yrare cascades. Hence there is a greater sensitivity to background subtraction and, as noted in [7], contaminant lines. One way to check the line-shape fitting (and hence the reliability of the centroid shift method) is to use another technique to measure the Q_0 of these bands. A coincidence recoil distance method (RDM) experiment has been performed for ^{133}Nd, and preliminary analysis [40] indicates that it will be possible to measure the lifetimes of the five states which decay via the 683-, 603-, 513-, 441-, and 409/344-keV transitions. The results obtained from this experiment will in principle be free of any dependence on stopping powers and sidefeeding. Hence, it should be possible to obtain the lifetime of the state which decays via the 683-keV transition using both methods, which will provide any extremely useful check on the DSAM.

V. SUMMARY AND CONCLUSIONS

In summary, the quadrupole moments of the highly deformed bands in ^{133}Nd and ^{137}Nd have been measured using the Doppler-shift attenuation method. Values of $(6.0\pm0.7)e$ b and $(4.0\pm0.5)e$ b, respectively, have been extracted from a centroid shift analysis, corresponding to axial prolate deformations of $\beta_2\simeq0.33$ and $\simeq0.22$. A line-shape analysis has also been carried for ^{133}Nd which gave a slightly larger value of $Q_0=(\underline{6.7}\pm0.7)e$ b with slower sidefeeding corresponding to $Q_{sf}=5.3e$ b. This gave a slightly larger deformation of $\beta_2\simeq0.37$. Total Routhian surface (TRS) calculations predict a prolate minimum with a deformation of $\beta_2=0.36$–0.34 over the range of rotational frequencies where the band in ^{133}Nd is observed. Hence, there is good agreement between the experimental and theoretical deformations.

In the case of ^{137}Nd, the TRS calculations predict a triaxial minimum with $\beta_2=0.27$ and $\gamma\sim10°$–$20°$, which moves into a prolate minimum ($\beta_2=0.29$, $\gamma=3°$–$5°$). Cranked shell model calculations indicate that the alignment of a pair of $h_{9/2}$ neutrons drives the nucleus to the triaxial shape. This nonaxial shape can explain the low Q_0 ($4e$ b) of the band at high rotational frequencies ($\hbar\omega>0.5$ MeV), but a larger Q_0 would be expected below the band crossing, since the shape is now predicted to be prolate. In this scenario, the unique second humplike feature in the $\mathcal{J}^{(2)}$ moment of inertia can (at least in part) be attributed to the $h_{9/2}$ neutron alignment. The CSM calculations also predict a contribution from the alignment of $h_{11/2}$ neutrons. An alternative scenario would be that the band is based on an $h_{9/2}$ neutron, with a smaller

deformation than the $i_{13/2}$ configuration.

The results for ^{133}Nd and ^{137}Nd form part of a systematic body of data which has been gathered concerning quadrupole moments of highly deformed bands in the light rare-earth region. The deformations inferred from the Q_0 measurements vary between nuclei, which suggests that the dominant deformation driving force is the single-particle configuration, rather than "stabilization" from shell gaps in a deformed potential. Differences of $\sim 10\%$ in Q_0, either between bands in different nuclei or a variation along one band, are at the limit of the reliability of the investigations discussed here. State-of-the-art calculations predict such variations, so it clear that an improvement in the experimental technique is needed if the theories are to be tested to the fullest of their predictive power.

One immediate way is to remove the effect of sidefeeding on the analysis. This can be done by "gating above" the transitions of interest, but for such weak bands the statistics required to do this would be enormous. However, the next generation of γ spectrometers such as EUROGAM and GAMMASPHERE, should be able to provide this requirement.

The lack of knowledge on the stopping powers, particularly the nuclear component and the associated scattering, is a more difficult problem to overcome. Extensive measurements of stopping powers, or an improvement on the Lindhard theory, do not seem likely. The use of an inverse reaction to give a higher initial recoil velocity would help to lessen the sensitivity to the nuclear stopping. This would bring the disadvantage of much broader peaks, and also the possibility of the "normal deformed" peaks showing Doppler shifts, which would result in very complex spectra. If, however, this latter problem is not serious, then combining an inverse reaction with EUROGAM or GAMMASPHERE may be the next step in improving the sensitivity of DSAM measurements.

This work was supported by the UK Science and Engineering Research Council, who provided financial support for S.M.M., J.R.H., and I.J. Funding for Y.J.H. was supplied the British Council Exchange scheme. R.A.W. acknowledges support from the Swedish Natural Research Council and the Sweden America Foundation. We wish to thank the crew and staff at the Daresbury NSF for supplying the beams and miscellaneous support. We also thank A. G. Smith (Manchester) for supplying the new line-shape fitting code, and C. W. Beausang for helpful discussions.

[1] S. M. Polikanov, V. A. Druin, V. A. Karnaukhov, V. L. Mikheev, A. A. Pleve, N. K. Skobelev, V. G. Subbotin, G. M. Ter-Akop'yan, and V. A. Fomichev, Zh. Eksp. Teor. Fiz. **42**, 1464 (1962) [Sov. Phys. JETP **15**, 1016 (1962)].

[2] P. J. Nolan, A. Kirwan, D. J. G. Love, A. H. Nelson, D. J. Unwin, and P. J. Twin, J. Phys. G **11**, 217 (1985).

[3] A. J. Kirwan, Ph.D. thesis, University of Liverpool, UK 1986; and unpublished.

[4] A. J. Kirwan, P. J. Bishop, D. J. G. Love, D. J. Thornley, A. Dewald, A. Gelberg, K. Schiffer, and K. O. Zell, J. Phys. G **15**, 85 (1989).

[5] A. J. Kirwan, G. C. Ball, P. J. Bishop, M. J. Godfrey, P. J. Nolan, D. J. Thornley, D. J. G. Love, and A. H. Nelson, Phys. Rev. Lett. **58**, 467 (1987).

[6] Y-J. He, M. J. Godfrey, I. Jenkins, A. J. Kirwan, P. J. Nolan, S. M. Mullins, R. Wadsworth, and D. J. G. Love, J. Phys. G **16**, 657 (1990).

[7] R. M. Diamond, C. W. Beausang, A. O. Macchiavelli, J. C. Bacelar, J. Burde, M. A. Deleplanque, J. E. Draper, C. Duyar, R. J. McDonald, and F. S. Stephens, Phys. Rev. C **41**, R1327 (1990).

[8] P. H. Regan *et al.*, Phys. Rev. C **42**, R1805 (1990).

[9] E. S. Paul *et al.*, J. Phys. G **18**, 121 (1992).

[10] T. K. Alexander and J. S. Forster, in *Advances in Nuclear Physics,* edited by Michel Baranger and Erich Vogt (Plenum, New York, 1978), Vol. 10, Chap. 3.

[11] J. F. Sharpey-Schafer and J. A. Simpson, *Progress in Particle and Nuclear Physics,* edited by Amand Faessler (Pergamon, Oxford, 1988), Vol. 21, Chap. 7, p. 293.

[12] P. J. Nolan, in *Proceedings of the International Nuclear Physics Conference,* Harrogate, UK, edited by J. L. Durell, J. M. Irvine, and G. C. Morrison, IOP Conference Series Number 86 (IOP, Bristol, 1986), Vol. 2, p. 155.

[13] R. Wadsworth, *et al.*, J. Phys. G **13**, L207 (1987).

[14] S. M. Mullins, D. Phil thesis, University of York, UK 1989.

[15] I. Jenkins, Ph.D. thesis, University of Liverpool, UK 1990.

[16] D. J. G. Love, private communication.

[17] K. Braune, MPI Heidelberg Diploma, 1977; D. Pelte and D. Schwalm, in *Heavy Ion Collisions,* edited by R. Bock (North Holland, Amsterdam, 1982), Vol. 3, Chap. 1.

[18] J. F. Ziegler, *Handbook of Stopping Cross Sections for Energetic Ions in All Elements* (Pergamon, New York, 1980).

[19] J. F. Ziegler and J. P. Biersack, in *Treatise on Heavy-Ion Science,* edited by D. A. Bromley (Plenum, New York, 1985), Vol. 6, Chap. 3.

[20] A. E. Blaugrund, Nucl. Phys. **88**, 501 (1966).

[21] J. C. Bacelar, unpublished.

[22] J. Gascon *et al.*, Nucl. Phys. **A513**(2), 344 (1990).

[23] J. Lindhard, M. Scharff, and H. E. Schiøtt, Kgl. Dan. Vidensk. Selsk. Mat. Fys. Medd. **33**, 14 (1963).

[24] E. F. Moore *et al.*, Phys. Rev. Lett. **64**, 3127 (1990).

[25] K. E. G. Löbner, M. Vetter, and V. Honig, Nucl. Data Tables A **7**, 495 (1970).

[26] T. Bengtsson, NORDITA Report No. 87/14N, 1987.

[27] R. A. Wyss, J. Nyberg, A. Johnson, R. Bengtsson, and W. Nazerewicz, Phys. Lett. **215B**, 211 (1988).

[28] M. J. Godfrey, Y. He, I. Jenkins, A. Kirwan, P. J. Nolan, R. Wadsworth, and S. M. Mullins, J. Phys. G **15**, L163 (1989).

[29] E. M. Beck, R. J. McDonald, A. O. Macchiavelli, J. C. Bacelar, M. A. Deleplanque, R. M. Diamond, J. E. Draper, and F. S. Stephens, Phys. Lett. **195B**, 531 (1987).

[30] R. Ma, E. S. Paul, C. W. Beausang, S. Shi, N. Xu, and D. B. Fossan, Phys. Rev. C **36**, 2322 (1987).

[31] J. Nyberg *et al.*, Liverpool Nuclear Structure Group Biannual Report 1989/1990, p. 29.

[32] S. M. Mullins *et al.*, unpublished.

[33] J. Nyberg, presented at the Workshop on Nuclear Struc-

ture at High Spins, Bad Honnef, West Germany, 1989 (unpublished).
[34] L. Hildingsson *et al.*, Nucl. Phys. **A513**, 394 (1990).
[35] P. H. Regan *et al.*, J. Phys. G (to be published).
[36] K. Schiffer, B. Herskind, and J. Gascon, Z. Phys. A **332**, 17 (1989).
[37] S. Juutinen *et al.*, Z. Phys. A **338**, 365 (1991).
[38] J. Simpson, H. Timmers, M. A. Riley, T. Bengtsson, M. A. Bentley, F. Hanna, S. M. Mullins, J. F. Sharpey-Schafer, and R. Wyss, Phys. Lett. **262B**, 388 (1991).
[39] Y. Liang *et al.*, Phys. Rev. C **44**, R578 (1991).
[40] S. A. Forbes, private communication and unpublished.

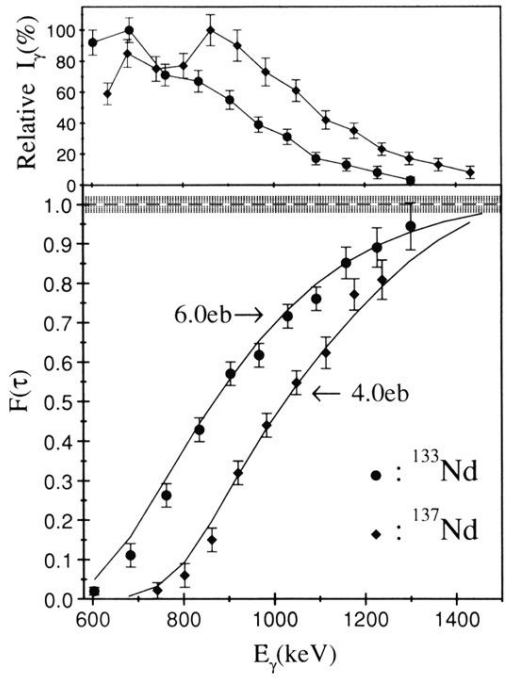

FIG. 2. Bottom: Experimental $F(\tau)$ values extracted from the Doppler-shifted peaks. The dotted region indicates the estimates spread in initial recoil velocity due to the $\sim$500-μg/cm^2 thickness of the targets used in the experiments. The curves assume a single cascade which has a constant quadrupole moment. Any sidefeeding has been assumed to have the same time structure as the inband feeding. Top: Feeding patterns from the unbacked target data. These show the relative intensities of the in-band transitions when gating on the same transitions as were used in the backed target data.

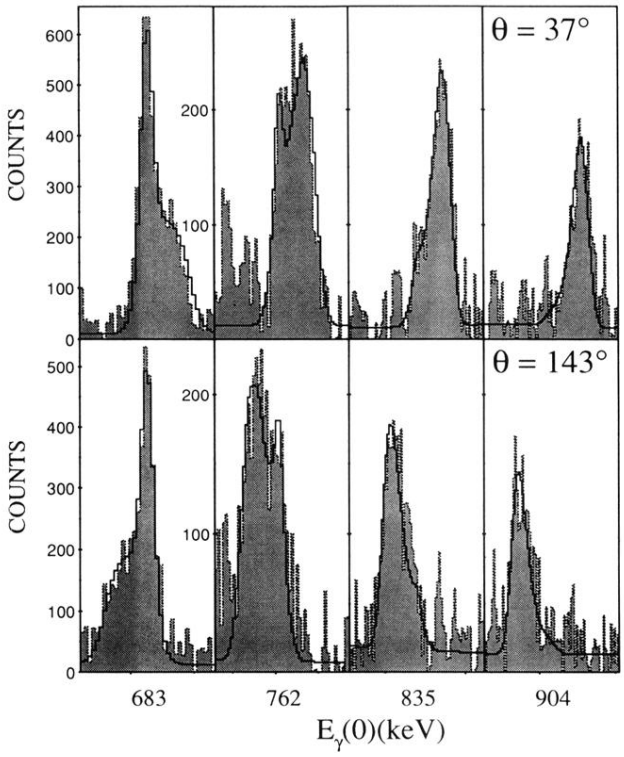

FIG. 3. Comparison of calculated line shapes (solid lines) with experiment (dotted lines and shaded-in area) for the 683-, 762-, 835-, and 904-keV transitions in ^{133}Nd. Details of how the fits were produced are described in the text. Transitions below 683 keV were fully stopped, and hence displayed no line shape, while those above 904 keV were relatively insensitive to the fitting procedure.